Sensing, Switching and Modulating Applications of a Superconducting THz Metamaterial

Zohreh Vafapour, *Member, IEEE*, Mitra Dutta, *Life Fellow, IEEE*, and Michael A. Stroscio, *Life Fellow, IEEE*

***Abstract*—The emergence of planar metamaterials (PrMMs) has opened a gateway to unprecedented electromagnetic (EM) properties and functionality unattainable from naturally occurring materials, thus enabling a family of PrMM based devices. In this paper, a novel class of superconducting (SC) PrMM is presented and a series of THz reflectance spectral responses simulations reveals that these SC PrMM structures portend applications in a variety of temperature sensors, thermo-optical modulators, and magnetic switch devices.**

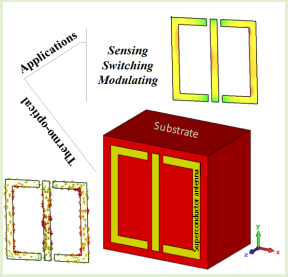

***Index Terms*—Superconducting metamaterial, plasmonic waveguide, temperature sensing, magnetic switching application, thermo-optical modulating application.**

I. Introduction

SUPERCONDUCTING (SC) terahertz (THz) metamaterials (MMs) have attracted significant interest due to low loss, efficient resonance switching and large range frequency tunability. At low temperatures, SC materials possess superior conductivity relative to metals at frequencies up to the THz range, and therefore it is expected that SC MMs will have a lower loss than metal MMs. There have been a few recent demonstrations of SC MMs, which are of interest in loss reduction and resonance tuning [1], [2]. Recent studies show using vanadium oxide-based metamaterial in modulating, sensing, and active filtering applications [3]. In 2008, L Kang, et al proposed a design using ferrite-based metamaterial which has the ability to use in cloaking applications [4]. The other interesting research on SC MMs investigated the EIT-like phenomenon [5] and THz device applications using SC metamaterial [6], [7]. The superconductivity in the MMs dramatically reduces ohmic loss and absorption to levels suitable for novel devices such as modulators [8]–[10], switches [11], [12], sensors [13]–[17], slow light devices [5], [18]–[21] over a broad range of the electromagnetic (EM) spectrum.

Planar metamaterials (PrMMs) are very thin material films that are patterned on a subwavelength scale [22]–[25]. The emergence of planar metamaterials has opened a gateway to unprecedented electromagnetic properties and functionality unattainable from naturally occurring materials, thus enabling a family of PrMM based devices such as biosensors [26]–[33], biomedical detectors [34]–[36], optical non-linear liquid sensors [37]–[40], chemical sensors [41]–[43], glucose sensors [44], [45], slow light devices [46]–[49], optical buffering [50], [51], modulator devices [52]–[54], super lenses [55], [56], cloak designs [57], [58], and switches [59], [60]. The response of PrMMs can also be engineered to mimic EM response in all frequency regimes such as visible [61]–[64], near-infrared [39], [40], [45], [65]–[68], mid- infrared [59]–[72], far-infrared [73]–[75], and THz [41], [47], [7], [77]–[80].

In the context of the present work, the property that matters most is showing the tunability of the proposed design. First, we look at the THz transmittance spectral responses to investigate changes in resonant frequency/wavelength of the proposed SC PrMM in different cases through optical, material, geometrical, thermal, and magnetic tuning. Here, we systematically elaborate numerical demonstrations of the proposed SC PrMM, the tuning behaviors of their resonance performance, and theoretical understanding of its unique performance based on analyzing the EM field distributions and surface currents. In the last part of this paper, by looking at

Manuscript received March 25, 2021; accepted April 11, 2021. Date of publication April 13, 2021; date of current version June 30, 2021. The associate editor coordinating the review of this article and approving it for publication was Dr. M. Jaleel Akhtar. *(Corresponding author: Zohreh Vafapour.)*

Zohreh Vafapour is with the Department of Electrical and Computer Engineering, University of Illinois at Chicago, Chicago, IL 60607 USA, and also with the Department of Bioengineering, University of Illinois at Chicago, Chicago, IL 60607 USA (e-mail: z.vafapour@gmail.com; zvafa@uic.edu).

Mitra Dutta is with the Department of Electrical and Computer Engineering, University of Illinois at Chicago, Chicago, IL 60607 USA, and also with the Department of Physics, University of Illinois at Chicago, Chicago, IL 60607 USA.

Michael A. Stroscio is with the Department of Electrical and Computer Engineering, University of Illinois at Chicago, Chicago, IL 60607 USA, also with the Department of Bioengineering, University of Illinois at Chicago, Chicago, IL 60607 USA, and also with the Department of Physics, University of Illinois at Chicago, Chicago, IL 60607 USA.

Digital Object Identifier 10.1109/JSEN.2021.3073078

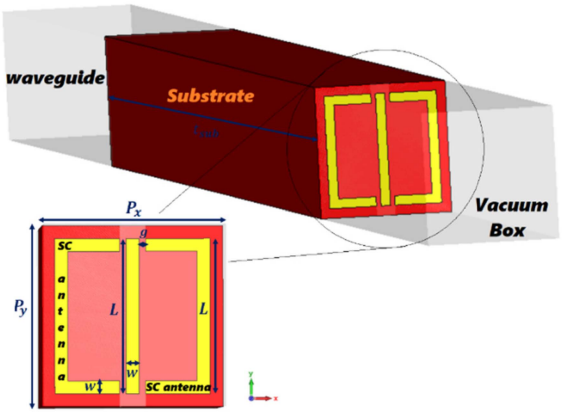

Fig. 1. The 3D-, and 2D- view of the unit cell schematic of the perfect absorber nanostructure created by the CST simulator.

the THz reflectance spectral responses, we show the proposed design has the potential applications as a temperature sensor, thermo-optical modulator, and magnetic switch device.

II. Structure Description

The sample is made of a square array of split ring resonator (SRR) antenna plus a cut wire antenna as shown in Fig. 1. In fact, we split the SRR in to two different parts and placed the cut wire antenna between them. The cut wire antenna has a length of $l = 60\,\mu m$ with the width of $w = 5\,\mu m$. The geometrical parameters of the square SRR are as follow: $L = 60\,\mu m, W = 5\,\mu m$, while the gap between the left and right parts of square SRR with the cut wire is $g = 2.5\,\mu m$. All three of these antennas are made of Niobium Nitride (NbN) which is a SC material and located on a dielectric material which serves as a substrate. We use magnesium oxide or magnesia (MgO) as substrate in this design. The MgO is modelled as a lossless dielectric medium with relative permittivity of $\varepsilon_{MgO} = 11.5$, while NbN is simulated with a conductivity of $\sigma(\omega)$ which will be describe and calculated as follows. The other geometrical parameters are as follows: $t_{SC} = 0.2\,\mu m$, $t_{Sub} = 1000\,\mu m$, $P_X = P_Y = 70\,\mu m$. The complex conductivity of the SC PrMM thin film is formulated as [81]:

$$\sigma(\omega) = \sigma_r(\omega) + i\sigma_i(\omega), \tag{1}$$

According to the Maxwell-Garnet model, the conductivity of the SC NbN can be expressed as [81]:

$$\sigma(\omega) = \frac{2 f_n \sigma_{SC}(\sigma_n - \sigma_{SC})}{(1 - f_n)(\sigma_n - \sigma_{SC}) + 2\sigma_{SC}} + \sigma_{SC}, \tag{2}$$

in which, f_n is defined as the filling factor referring to the contributions of the SC and normal electrons to the conductivity [82] and formulated as:

$$f_n = \frac{n_n}{n_n + n_{SC}}, \tag{3}$$

Here, n_n is the density of normal electrons, n_{SC} is the density of SC electrons, and σ_n and σ_{SC} are defined as normal and SC carriers' conductivities, respectively. In accordance with a two-fluid model, there are two kinds of charge carriers in superconductors: normal carriers with conductivity of $\sigma_n(\omega)$ and SC carriers with conductivity of $\sigma_{SC}(\omega)$. Normal carriers are described by the Drude model as:

$$\sigma_n(\omega) = \frac{\sigma_0}{(1 - i\omega t)}, \tag{4}$$

in which, σ_0 is defined as the dc conductivity of the SC PrMM thin film and is equal to

$$\sigma_0 = \frac{n_n e^2 \tau}{m_0}, \tag{5}$$

where e is the electron charge, τ is the relaxation time, m_0 is the electron mass, and ω is the angular frequency of THz incident light which equals to $\boldsymbol{\omega} = 2\pi \mathrm{f}$, where f is the frequency of incident light. The conductivity of the SC carriers is given by the London equation as follows:

$$\sigma_{SC}(\omega) = i\frac{n_{SC} e^2 \tau}{m\omega} = i\frac{1}{\mu_0 \omega \lambda_L^2}, \tag{6}$$

where, $\lambda_L$is the London penetration depth, m is electron mass in SC, and μ_0 is the vacuum permeability.

The effective surface impedance of the SC thin film with thickness of t_{SC} is expressed as [1], [83], [84]

$$\begin{aligned} Z_{s,eff}(\omega) &= R_{s,eff} + jX_{s,eff} \\ &= \sqrt{\frac{j\omega\mu_0}{\sigma(\omega)}} \coth\left(t_{SC}\sqrt{j\omega\mu_0\sigma(\omega)}\right), \end{aligned} \tag{7}$$

in which $R_{s,eff}$ is the effective surface resistance and $X_{s,eff}$ is reactance which is calculated as follows:

$$X_{s,eff} = \omega L_K, \tag{8}$$

where, L_K is the kinetic inductance and μ_0 is the magnetic susceptibility in vacuum.

The wave propagates in the Z-direction, which is perpendicular to the plane of the SC PrMM, with the ac electric field parallel to the gap, i.e., in the X-direction, and the magnetic field is along the Y-direction, as shown in Fig. 1. The measured data in all figures are supported by full-wave numerical simulations using CST Microwave Studio simulator software. The unit cell shown in Figure 1(a) is reproduced in the simulations using periodic boundary conditions.

THz time domain experiments extend a unique prospect to explore fast nonlinear response in superconducting materials because the experiment involves a brief approximately picosecond (ps) single cycle THz bandwidth excitation of the metamaterial. The structures were formed in Niobium Nitride films deposited on Magnesium oxide material with thickness of 1000 micrometer as a substrate. It was found that an intense THz pulse on a NbN metamaterial could produce significant de-pairing, resulting in a large quasi-particle density and increase in effective surface resistance of the film. The NbN films typically have a critical temperature of 15.8K. If raising the temperature of NbN from 1.6 k to 15 K (see Fig. 4) at constant distance, the loss of the system will increase. While experimental progress in the superconducting metamaterial field is relatively new, the increasing amount of research over the last decade is an encouraging indicator that this field is moving forward quickly.

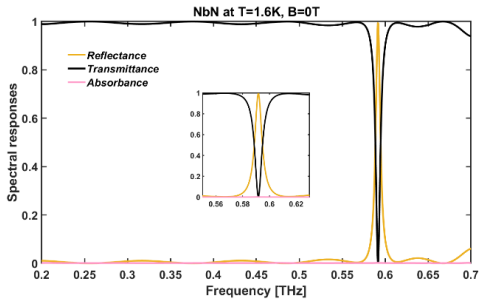

Fig. 2. Absorbance and other spectra.

III. Spectral Responses and Physical Concepts

An obvious transmission valley appears at about $f_{resonance} = 0.5915$ THz as shown in black curve in Fig. 2, which is a dip resonance in the spectral response. Corresponding to the dip transmission, there is a peak resonance in reflection spectrum represented by the yellow curve in Fig. 2. As can be seen from Fig. 2, the transmission coefficient at 0.5915 THz is about 0.48% and the reflection coefficient is about 99.23%; therefore, based on the formula used to calculate the absorption, i.e. A = 1-T-R, the absorption coefficient at 0.5915 THz is approximately 0.29%. The transmission ($t(\omega)$), and reflection ($r(\omega)$), and absorption ($a(\omega)$) coefficients are calculated as follows [85], [86]:

$$t(\omega) = \frac{1 + n_{sub}}{1 + n_{sub} + Z_0 \sigma(\omega) t_{SC}}, \tag{9}$$

$$r(\omega) = \frac{1 - n_{sub} - Z_0 \sigma(\omega) t_{SC}}{1 + n_{sub} + Z_0 \sigma(\omega) t_{SC}}, \tag{10}$$

$$a(\omega) = 1 - \frac{1 + n_{sub}}{1 + n_{sub} + Z_0 \sigma(\omega) t_{SC}} - \frac{1 - n_{sub} - Z_0 \sigma(\omega) t_{SC}}{1 + n_{sub} + Z_0 \sigma(\omega) t_{SC}}, \tag{11}$$

in which n_{sub} is the refractive index of the substrate, t_{SC} is thickness of the SC PrMM thin film, and Z_0 is the impedance in vacuum.

To reveal the underlying physical mechanism of the resonance existence, the EM field distributions and surface currents are quantitatively investigated in Fig. 3. At $f_{resonance} = 0.5915$ THz, the total electric field intensity distribution and surface current are shown in Fig. 3(a, b). It can be clearly seen that electric field is mainly confined along the cut wire NbN SC antennas and two electric dipole moments are created which causes the dip resonance in transmission spectrum. Furthermore, it is found that the electric fields are strong at the end of NbN SC cut wire antennas at X-Y plane as shown in Fig. 3a, which significantly increases the light-matter interaction and leads to a narrow transmission window at $f_{resonance}$. Figures 3c to 3f shows the magnetic field distributions and the magnetic surface currents. As can be seen from parts c to e of Fig.3, the localized surface plasmon resonance (LSPR) occurs and enhances the EM field at the left and right sides of the cut wire NbN SC antennas and confines the magnetic field among the Y-direction. Therefore, there is a strong magnetic field along the Y-direction in the SC antennas.

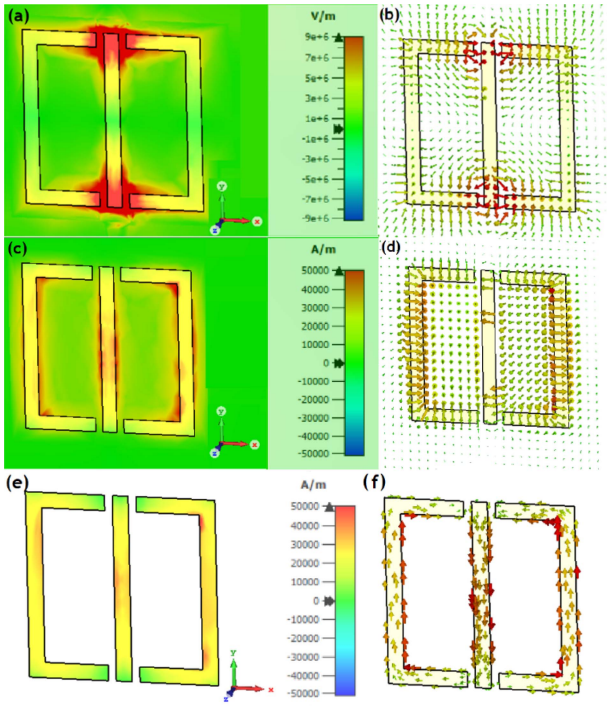

Fig. 3. Electric field (a) distributions; (b) Surface current; Magnetic field (c,e) distributions, (d,f) surface currents.

IV. Investigation of Tunability of the Microstructure

The control of the behavior of superconducting MMS, including resonance frequency shift and transmitted amplitude modulation, is especially interesting since the superconductivity exhibits a strong dependence on the ambient conditions. In the following, to elucidate the underlying tunability mechanism of the proposed THz SC PrMM, we compare the transmission spectra of the proposed microstructure by changing the thermal, optical, material, and geometrical parameters of the proposed microstructure design.

A. Magnetic Tunability

Figures 4(a) to 4(f) systematically show transmittance spectra versus frequency for different fixed temperatures; we have measured the THz responses of the proposed SC PrMM microstructure design under different magnetic field intensities. These figures show the measured transmission spectra as B varies from 0 to 7.0 T. Figure 4 shows the evolution of the measured amplitude transmission for different samples. It can be seen that by increasing the magnetic field at any fixed temperature, the transparency window is obviously broadened, and the sharp narrow transparency resonance dip is vanishing. By increasing the value of the magnetic field further to 5 T, the bandwidth of the transparency window is dramatically increased with a nearly flat resonance dip. At a low strength magnetic field of 0 T, the transmission shows a sharp resonance dip approaching approximately zero for the transmission coefficient. As the magnetic field is increased from 0 to 7.0 T, the resonance transmission dip increases from below 0.005 to more than 0.9 without a prominent resonance frequency shift.

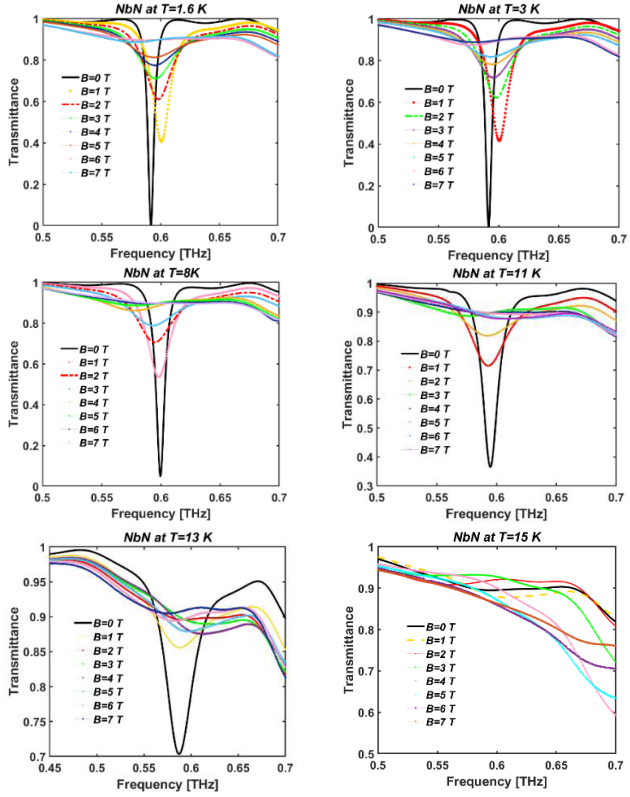

Fig. 4. Changing magnetic field at fixed temperature and effect on the spectra.

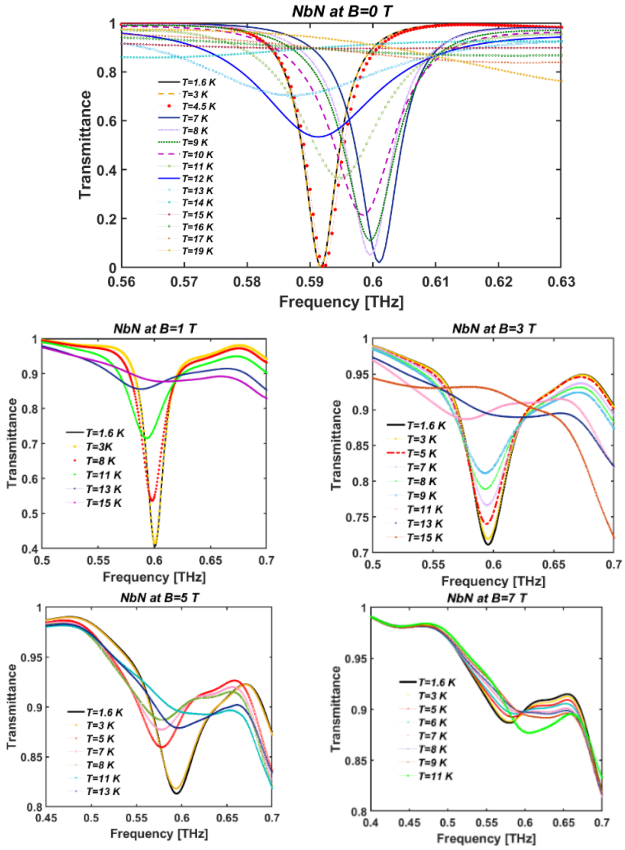

Fig. 5. Changing temperature of the SC PrMM and effect on the spectra.

At B = 7.0 T, the resonant dip is significantly weaker. Thus, a substantial change of more than 90% in the resonance transmission is achieved by increasing the magnetic field, indicating that the resonance properties of the SC resonators/antennas are strongly dependent on the magnetic field. When magnetic field is strong enough, superconductivity is quenched, and the SC elements are switched to the normal state. Therefore, this SC PrMM design allows us to simply switch between the low-transmission state and the high-transmission state by applying or removing the applied magnetic field. It should be noted that this behavior is typical in magnetic switching applications which will be investigated in this research in the application section.

B. Temperature Tunability

To show the temperature tunability capability/possibility of the proposed THz SC PrMM microstructure, we simulated the transmission spectra of the microstructure design at a fixed magnetic field by changing the temperature of the SC antennas. As can obviously be seen from Fig. 5, as temperature goes up above the critical temperature of $T_C = 13.8$ K, the transmission grows stronger due to the SC carriers. At temperatures lower than 13.8 K, there is a sharp transmission dip resonance in the transmission spectrum. At 19 K, as the temperature far above Tc, the NbN SC PrMM does not exhibit any resonance in the transmission spectrum, as represented the T_C value. The simulated amplitude transmission shown in Figs. 4(e) and 5(a) also demonstrates the switching effect at both the resonances as the temperature reaches to 13.8 K in the case of no magnetic field.

C. Optical Tunability

To further illustrate the optical tuning of the proposed SC PrMM microstructure, we investigated the transmission properties of the proposed design in different polarization modes and different angles of incident light in Figs. 6a, and b, respectively. The measured transmission of transverse electric (TE) and transverse magnetic (TM) polarization modes in Fig. 6a show distinct behavior over the THz frequency regime of operation of this microstructure. From Fig. 6(a), one can see the existence of the transmission resonance mode in the TE polarization mode (blue-line curve) which means that the SC antennas could couple with the normal incident light. But there is no resonance mode in the transmission spectrum of TM polarization mode (red-dashed-dotted curve).

The transmission can be actively controlled by adjusting the polarization angle and reaches dual band when the polarization is TE mode and the incident light was not illustrated as normal incident (i.e., $\theta \neq 0$). The proposed microstructure is effective in managing light transmission by using different polarization modes and angle of incident light. As can be seen from Fig. 6b, there is a plasmonically induced transparency (PIT) effect when the incident light is not in normal incident. As can be seen in Fig. 6b, there is a dual-band transmission spectrum which means that the higher order plasmonic modes are excited and the PIT effect is created. As is clearly observable from Fig. 6b, there is approximately a 99.91% transmission coefficient for the case of $\theta = 40°$ at about 0.59 THz which was less than 0.5% at normal incidence ($\theta = 90°$).

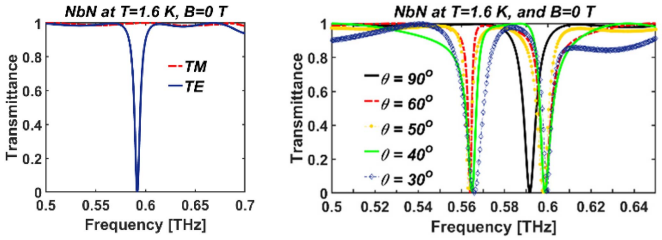

Fig. 6. Change (a) polarization, and (b) angle of incident light and their effects on the transmission spectra.

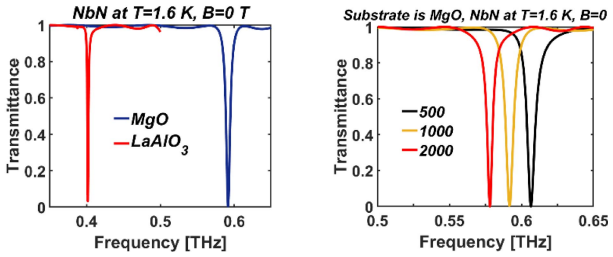

Fig. 7. Change substrate (a) material and (b) thickness and effect on the spectra (t_{sub} [μm]).

D. Material Tunability

Figure 7 shows the simulation results of the transmittance spectra using different substrate material and thickness. The transmittance resonance frequency red shifted by increasing/decreasing the RI of the substrate material from MgO ($\varepsilon_{MgO} = 11.5$) to lanthanum aluminate, which is denoted by $LaAlO_3$ or LAO ($\varepsilon_{LAO} = 24.5$) [87]. A clear red shift of the transmission resonance is observed due to the increase of the RI of the dielectric material used as a substrate. As can be seen in Fig. 7(a), the resonance frequency position depends very sensitively on the substrate material. Figure 7(b) shows the simulated transmittance spectra of the designed superconductor metamaterial for different thicknesses of a MgO substrate. As can be seen from Fig. 7(b), there is a blue shift by decreasing the thickness of substrate. As can be seen from Fig. 7(b), there is a blue shift by decreasing the thickness of substrate.

E. Geometrical Tunability

To further confirm the physical origin of the transmission spectrum and narrow transmission band, the influence of geometric parameters is investigated. As shown in Fig. 8(a), with other parameters fixed, when g changes from 0.5 to 5 μm, the transmission resonance dip become blue shifted, but the transmission strength remains unchanged. But as can be seen from Fig. 8a, in the case of g $=$ 0 μm, there is no resonance transmission dip due to the lack of coupling between SC antennas and normally incident light. Fig. 8(b) shows the effect of changing w from 1 to 15 μm while all other geometrical parameters are fixed; there is a blue shift by increasing w without any changes in the transmission resonance dip broadening. From Fig. 8(c), it is noted that the transmission resonance dip becomes redshifted by increasing the amount of the l parameter from 10 to 60 μm; also, the resonance transmission dip becomes narrow by increasing the amount of l.

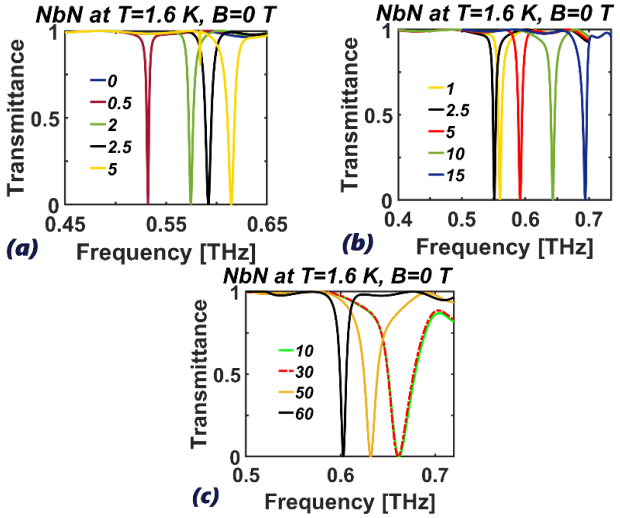

Fig. 8. Change geometrical parameters and effect on the transmission spectra (a) g [μm], (b) W [μm], and (c) l [μm].

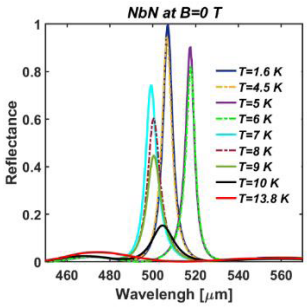

Fig. 9. Temperature-dependent reflection spectrum vs. wavelength at B $=$ 0 T.

V. Applications

Superconducting THz MMs have recently drawn great attention within the THz and MMs fields, due to their low ohmic loss as well as their thermal and magnetic-field tuning behavior [7], [8]. Based on the phenomena that SC depends on temperature and magnetic field, we investigated the temperature sensing, thermo-optical modulating, and magnetic switching applications of the proposed SC PrMM microstructure design.

A. Temperature Sensing Application

The reflection property of the proposed SC PrMM is simulated. In the simulation, the magnetic field is equal to zero, i.e., B $=$ 0 T using MgO as a substrate with normal incident light TE polarization. As can be seen from Fig. 9, the reflection spectrum experiences a frequency/wavelength shift by changing the temperature of the SC antennas. We demonstrate a temperature tuning of more than 33.3 μm within the temperature range limited by the critical temperature of the proposed SC PrMM material. A big resonance shift is observed as the temperature is decreased. We can use this capability in temperature sensing applications for the proposed SC PrMM device. This is due to the interplay of the temperature-dependent behavior of the SC material and the spectral responses. Thus, we demonstrate, thermal tuning of

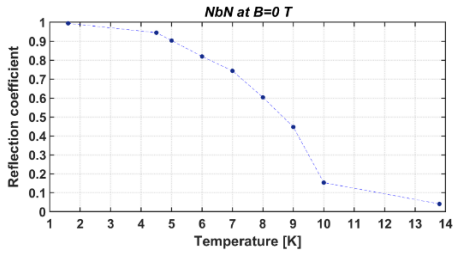

Fig. 10. The reflection coefficient values vs temperature at B = 0 T.

sensitivity which is entirely based on temperature dependence of the NbN SC material. The wavelength and frequency sensitivities, i.e., S_λ in the scale of [μm/K], and S_ω in units of [THz/K] are calculated in relations 12, and 13, respectively, as follows [88]:

$$S_\lambda = \left|\frac{\Delta\lambda}{\Delta T}\right| = \left|\frac{\lambda_{max} - \lambda_{min}}{\Delta T}\right|, \tag{12}$$

$$S_\omega = \left|\frac{\Delta\omega}{\Delta T}\right| = \left|\frac{\omega_{max} - \omega_{min}}{\Delta T}\right|, \tag{13}$$

As a result, the proposed SC PrMM microstructure design has a maximum temperature sensitivity of about 18.5 μm/K (corresponding to 2.15 $\times 10^{-2} THz/K$) which is an ultra-high sensitivity value in comparison to recently designed temperature sensors in the literature [59], [89]–[93] and can be used in many applications for accurate temperature detection.

B. Thermo-Optical Modulating Application

As the next step toward other multiplexed applications on temperature dependence of the proposed SC PrMM device, we investigate the thermo optic modulating applications of the proposed SC PrMM microstructure. As it is shown in Fig. 9, a "glossity bandwidth" appears in the proposed SC PrMM reflectance spectrum. Glossity bandwidth is defined as bandwidth between two reflection peak resonances in the reflectance spectrum. In the glossity bandwidth, there is a wavelength that has the highest reflection coefficient, and another has the lowest reflection coefficient, which refer to glossity wavelengths. The different of the two glossity wavelengths called the "glossity bandwidth". Here, the glossity wavelength at 1.6 K is about 507.2 μm (the maximum reflection coefficient at T = 1.6 K is about 0.9943), which decreases to 473.9 μm (the maximum reflection coefficient at T = 13.8 K is about 0.0408) by increasing the temperature of the SC PrMM to the critical value of $T_C = 13.8K$ (see Fig. 10). The "wavelength modulation depth" is defined as:

$$\lambda_{mod} = \frac{\Delta\lambda}{\lambda_{max}} = \frac{\lambda_{highest} - \lambda_{lowest}}{\lambda_{max}} = \frac{\lambda(T = 13.8K) - \lambda(T = 1.6K)}{\lambda_{max}}, \tag{14}$$

So, based on the relation 14, the wavelength modulation depth (λ_{mod}) percentage for the proposed SC PrMM is 6.56%. Moreover, based on temperature dependent changes the reflection coefficient values in the glossy bandwidths, we aim to

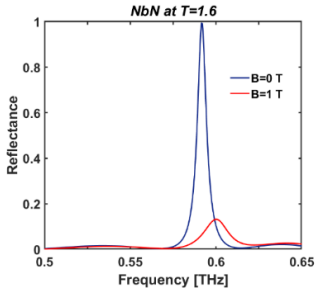

Fig. 11. The reflectance spectral responses vs frequency at fixed temperature of 1.6 K at different magnetic fields.

calculate "amplitude modulation depth" as follows:

$$R_{mod} = \frac{\Delta R}{R_{max}} = \frac{Refl.(T = 13.8K) - Refl.(T = 1.6K)}{Refl._{max}}, \tag{15}$$

As clearly observable from Fig. 9, by increasing the temperature from 1.6 K to the critical temperature of SC, of $T_C = 13.8K$, the reflection coefficient is decreased from 0.9943 to 0.0603. We achieve 95.9% for amplitude modulation depth (R_{mod}) of this device, which is an ultra-high value. Therefore, the proposed SC PrMM microstructure has great promise for thermo-optical plasmonic waveguide modulating applications in comparison to other superconductor structures in literatures [8]–[10].

C. Magnetic Switching Application

Here, we aim to show the proposed SC PrMM design is an outstanding candidate for magnetic switching applications in the THz frequency range. There are frequency/wavelength and spectral response changes caused by changing the magnetic field which is applied to the structure. At a fixed temperature and frequency, we define two different states as "ON" and "OFF" and calculate the modulation depth. When no magnetic field (B = 0 T) applied to the SC PrMM microstructure design, the reflection coefficient exhibits a maximum value of 0.9943 at the fixed temperature of 1.6 K. We called this situation as "ON" state. But, by increasing the magnetic field to B = 1 T, there is a low reflection coefficient about 0.063 in reflection spectrum which is defined as "OFF" state. According to the result in Fig. 11, once we set a higher value for magnetic field, we are in the OFF state and by removing the applied magnetic field, we are in the ON state. At a fixed temperature of 1.6 K and frequency of 0.5915 THz. We calculate the modulation depth [90] as follow:

$$\%MD_{switch} = \left|\frac{Refl.(ON) - Refl.(OFF)}{max\langle Refl.(ON), Refl.(OFF)\rangle}\right| \times 100 \tag{16}$$

We achieve 93.1% modulation depth which is an outstanding value in comparison to the reported literature so far [11], [12], [47], [59], [94], [95].

We also calculated the modulation efficiency (ME) based on the following relation [94]:

$$ME_{switch} = \left|\frac{10 \times \log\left[Refl.(ON)/Refl.(OFF)\right]}{B_{ON} - B_{OFF}}\right|, \tag{17}$$

which is about 12 dB/T. This switch device exhibits wide frequency operating ranges of optical bandwidth by applying an appropriate magnetic field. There has been a dynamic/active tunable control of modulation depth and efficiency by appropriately tuning the magnetic field, which holds great promise for application in future dynamic switching devices.

VI. Future Directions and Conclusion

Planar metamaterials (PrMMs) have shown promise for applications as biosensors, biomedical detectors, optical nonlinear liquid sensors, chemical sensors, glucose sensors, slow light devices, optical buffering, modulator devices, super lenses, cloak designs, and switches. In this paper, a novel class of superconducting (SC) PrMM is presented and a series of THz reflectance spectral responses simulations reveals that these SC PrMM structures portend applications in a variety of temperature sensors, thermo-optical modulators, and magnetic switch devices. Our simulations demonstrate that a new generation of SC PrMM devices can be expected to have improved device performance since it is found that: the resonance properties of the SC resonators/antennas are strongly dependent on the magnetic field suggestion applications in magnetic field sensing; there is an ultra-high modulation depth suitable for exploitation in thermo-optical plasmonic waveguide modulating applications; and the reflection spectrum exhibits an ultra-high sensitivity to temperature which provides a means of accurate temperature detection. These findings portend a wide range of future high-sensitivity sensors based on the novel SC PrMM introduced in this paper.

Acknowledgment

The authors declare no conflicts of interest. There is no funding to do this research.

References

[1] H. T. Chen *et al.*, "Tuning the resonance in high-temperature superconducting terahertz metamaterials," *Phys. Rev. Lett.*, vol. 105, no. 24, 2010, Art. no. 247402.

[2] P. Jung, A. V. Ustinov, and S. M. Anlage, "Progress in superconducting metamaterials," *Superconductor Sci. Technol.*, vol. 27, no. 7, 2014, Art. no. 073001.

[3] Z. Song, K. Wang, J. Li, and Q. H. Liu, "Broadband tunable terahertz absorber based on vanadium dioxide metamaterials," *Opt. Exp.*, vol. 26, no. 6, pp. 7148–7154, Mar. 2018.

[4] L. Kang, Q. Zhao, H. Zhao, and J. Zhou, "Magnetically tunable negative permeability metamaterial composed by split ring resonators and ferrite rods," *Opt. Exp.*, vol. 16, no. 12, pp. 8825–8834, 2008.

[5] C. Zhang *et al.*, "Tunable electromagnetically induced transparency from a superconducting terahertz metamaterial," *Appl. Phys. Lett.*, vol. 110, no. 24, Jun. 2017, Art. no. 241105.

[6] J. Wu *et al.*, "Tuning of superconducting niobium nitride terahertz metamaterials," *Opt. Exp.*, vol. 19, no. 13, pp. 12021–12026, 2011.

[7] B. B. Jin *et al.*, "Low loss and magnetic field-tunable superconducting terahertz metamaterial," *Opt. Exp.*, vol. 18, no. 16, pp. 17504–17509, 2010.

[8] J. Gu *et al.*, "Terahertz superconductor metamaterial," *Appl. Phys. Lett.*, vol. 97, no. 7, 2010, Art. no. 071102, doi: 10.1063/1.3479909.

[9] V. Savinov, V. A. Fedotov, S. M. Anlage, P. A. J. D. Groot, and N. I. Zheludev, "Modulating sub-THz radiation with current in superconducting metamaterial," *Phys. Rev. Lett.*, vol. 109, no. 24, 2012, Art. no. 243904.

[10] C. Li *et al.*, "Electrical dynamic modulation of THz radiation based on superconducting metamaterials," *Appl. Phys. Lett.*, vol. 111, no. 9, 2017, Art. no. 092601.

[11] Y. K. Srivastava *et al.*, "A superconducting dual-channel photonic switch," *Adv. Mater.*, vol. 30, no. 29, 2018, Art. no. 1801257.

[12] C. Kurter *et al.*, "Switching nonlinearity in a superconductor-enhanced metamaterial," *Appl. Phys. Lett.*, vol. 100, no. 12, 2012, Art. no. 121906.

[13] V. A. Fedotov *et al.*, "Temperature control of Fano resonances and transmission in superconducting metamaterials," *Opt. Exp.*, vol. 18, no. 9, pp. 9015–9019, 2010.

[14] V. Savinov, V. A. Fedotov, P. A. D. Groot, and N. I. Zheludev, "Radiation-harvesting resonant superconducting sub-THz metamaterial bolometer," *Superconductor Sci. Technol.*, vol. 26, no. 8, 2013, Art. no. 084001.

[15] I. Kawayama, C. Zhang, H. Wang, and M. Tonouchi, "Study on terahertz emission and optical/terahertz pulse responses with superconductors," *Superconductor Sci. Technol.*, vol. 26, no. 9, 2013, Art. no. 093002.

[16] S. Cibella *et al.*, "A metamaterial-coupled hot-electron-bolometer working at THz frequencies," *Proc. SPIE*, vol. 10103, Feb. 2017, Art. no. 101031M.

[17] Y. Kim *et al.*, "Single-layer metamaterial bolometer for sensitive detection of low-power terahertz waves at room temperature," *Optics Exp.*, vol. 28, no. 12, pp. 17143–17152, 2020.

[18] W. Cao, R. Singh, C. Zhang, J. Han, M. Tonouchi, and W. Zhang, "Plasmon-induced transparency in metamaterials: Active near field coupling between bright superconducting and dark metallic mode resonators," *Appl. Phys. Lett.*, vol. 103, no. 10, 2013, Art. no. 101106.

[19] B. B. Jin *et al.*, "Enhanced slow light in superconducting electromagnetically induced transparency metamaterials," *Superconductor Sci. Technol.*, vol. 26, no. 7, 2013, Jan. 074004.

[20] Y. Zhang, C. Li, and X. Tu, "Tuning electromagnetically induced transparency of superconducting metamaterial analyzed with equivalent circuit approach," *Prog. Electromagn. Res.*, vol. 91, pp. 29–37, 2020.

[21] M. Mirhosseini *et al.*, "Superconducting metamaterials for waveguide quantum electrodynamics," *Nature Commun.*, vol. 9, no. 1, pp. 1–7, 2018.

[22] N. Liu *et al.*, "Planar metamaterial analogue of electromagnetically induced transparency for plasmonic sensing," *Nano Lett.*, vol. 10, no. 4, pp. 1103–1107, 2010.

[23] Z. Vafapour, "Large group delay in a microwave metamaterial analog of electromagnetically induced reflectance," *J. Opt. Soc. Amer. A, Opt. Image Sci.*, vol. 3, no. 3, pp. 417–422, 2018.

[24] J. Wang *et al.*, "A novel planar metamaterial design for electromagnetically induced transparency and slow light," *Opt. Exp.*, vol. 21, no. 21, pp. 25159–25166, 2013.

[25] Z. Vafapour and H. Alaei, "Subwavelength micro-antenna for achieving slow light at microwave wavelengths via electromagnetically induced transparency in 2D metamaterials," *Plasmonics*, vol. 12, no. 5, pp. 1343–1352, 2017.

[26] A. I. Aristov *et al.*, "Laser-ablative engineering of phase singularities in plasmonic metamaterial arrays for biosensing applications" *Appl. Phys. Lett.*, vol. 104, no. 7, 2014, Art. no. 071101.

[27] A. Pal, A. Mehta, M. E. Marhic, K. C. Chan, and K. S. Teng, "Microresonator antenna for biosensing applications," *Micro Nano Lett.*, vol. 6, no. 8, pp. 665–667, 2011.

[28] A. A. Jamali and B. Witzigmann, "Plasmonic perfect absorbers for biosensing applications," *Plasmonics*, vol. 9, no. 6, pp. 1265–1270, 2014.

[29] W. A. Paiva-Marques, F. R. Gómez, O. N. Oliveira, and J. R. Mejía-Salazar, "Chiral plasmonics and their potential for point-of-care biosensing applications," *Sensors*, vol. 20, no. 3, p. 944, 2020.

[30] M. Ghasemi, N. Roostaei, F. Sohrabi, S. M. Hamidi, and P. K. Choudhury, "Biosensing applications of all-dielectric SiO_2-PDMS meta-stadium grating nanocombs," *Opt. Mater. Exp.*, vol. 10, no. 4, pp. 1018–1033, 2020.

[31] M. Bakır, M. Karaaslan, E. Unal, O. Akgol, and C. Sabah, "Microwave metamaterial absorber for sensing applications," *Opto-Electron. Rev.*, vol. 25, no. 4, pp. 318–325, 2017.

[32] P. Nie, D. Zhu, Z. Cui, F. Qu, L. Lin, and Y. Wang, "Sensitive detection of chlorpyrifos pesticide using an all-dielectric broadband terahertz metamaterial absorber," *Sens. Actuators B, Chem.*, vol. 307, Mar. 2020, Art. no. 127642.

[33] A. Danilov *et al.*, "Ultra-narrow surface lattice resonances in plasmonic metamaterial arrays for biosensing applications," *Biosensors Bioelectron.*, vol. 104, pp. 102–112, May 2018.

[34] A. Dolatabady, N. Granpayeh, and M. Abedini, "Nanoscale plasmonic detector of wave intensity difference and uni-directional waveguide," *Opt. Quantum Electron.*, vol. 51, no. 7, p. 230, 2019.

[35] Z. Vafapour, A. Keshavarz, and H. Ghahraloud, "The potential of terahertz sensing for cancer diagnosis," *Heliyon*, vol. 6, no. 12, 2020, Art. no. e05623.

[36] B. Choudhury, A. Menon, and R. M. Jha, "Active terahertz metamaterial for biomedical applications," in *Active Terahertz Metamaterial for Biomedical Applications*. Singapore: Springer, 2016, pp. 1–41.

[37] M. R. Forouzeshfard, S. Ghafari, and Z. Vafapour, "Solute concentration sensing in two aqueous solution using an optical metamaterial sensor," *J. Luminescence*, vol. 230, Feb. 2020, Art. no. 117734, doi: 10.1016/j.jlumin.2020.117734.

[38] Y. I. Abdulkarim, L. Deng, O. Altintas, E. Ünal, and M. Karaaslan, "Metamaterial absorber sensor design by incorporating swastika shaped resonator to determination of the liquid chemicals depending on electrical characteristics," *Physica E, Low-Dimensional Syst. Nanostruct.*, vol. 114, Oct. 2019, Art. no. 113593.

[39] E. S. Lari, Z. Vafapour, and H. Ghahraloud, "Optically tunable triple-band perfect absorber for nonlinear optical liquids sensing," *IEEE Sensors J.*, vol. 20, no. 7, pp. 10130–10137, Sep. 2020, doi: 10.1109/JSEN.2020.2989742.

[40] R. Kowerdziej and L. Jaroszewicz, "Tunable dual-band liquid crystal based near-infrared perfect metamaterial absorber with high-loss metal," *Liquid Cryst.*, vol. 46, no. 10, pp. 1568–1573, 2019.

[41] Z. Vafapour and H. Ghahraloud, "Semiconductor-based far-infrared biosensor by optical control of light propagation using THz metamaterial," *J. Opt. Soc. Amer. B, Opt. Phys.*, vol. 35, no. 5, pp. 1192–1199, 2018.

[42] Y. I. Abdulkarim *et al.*, "The detection of chemical materials with a metamaterial-based sensor incorporating oval wing resonators," *Electronics*, vol. 9, no. 5, p. 825, 2020.

[43] Z. Vafapour, "Near infrared biosensor based on classical electromagnetically induced reflectance (Cl-EIR) in a planar complementary metamaterial," *Opt. Commun.*, vol. 387, pp. 1–11, Mar. 2017.

[44] J. Vrba, D. Vrba, L. Díaz, and O. Fiser, "Metamaterial sensor for microwave non-invasive blood glucose monitoring," in *World Congress on Medical Physics and Biomedical Engineering 2019*. Singapore: Springer, 2018, pp. 789–792.

[45] Z. Vafapour, "Polarization-independent perfect optical metamaterial absorber as a glucose sensor in food industry applications," *IEEE Trans. Nanobiosci.*, vol. 18, no. 4, pp. 622–627, Oct. 2019.

[46] N. Papasimakis and N. I. Zheludev, "Metamaterial-induced transparency: Sharp Fano resonances and slow light," *Opt. Photon. News*, vol. 20, no. 10, pp. 22–27, 2009.

[47] Z. Vafapour, "Slowing down light using terahertz semiconductor metamaterial for dual-band thermally tunable modulator applications," *Appl. Opt.*, vol. 57, no. 4, pp. 722–729, 2018.

[48] J. Gu *et al.*, "Active control of electromagnetically induced transparency analogue in terahertz metamaterials," *Nature Commun.*, vol. 3, no. 1, pp. 1–6, 2012.

[49] Q. Bai, C. Liu, J. Chen, C. Cheng, M. Kang, and H. T. Wang, "Tunable slow light in semiconductor metamaterial in a broad terahertz regime," *J. Appl. Phys.*, vol. 107, no. 9, 2010, Art. no. 093104.

[50] H. Hu, D. Ji, X. Zeng, K. Liu, and Q. Gan, "Rainbow trapping in hyperbolic metamaterial waveguide," *Sci. Rep.*, vol. 3, no. 1, p. 1249, 2013.

[51] D. K. Hunter, M. C. Chia, and I. Andonovic, "Buffering in optical packet switches," *J. Lightw. Technol.*, vol. 16, no. 12, pp. 2081–2094, Dec. 1998.

[52] H. T. Chen, W. J. Padilla, M. J. Cich, A. K. Azad, R. D. Averitt, and A. J. Taylor, "A metamaterial solid-state terahertz phase modulator," *Nature Photon.*, vol. 3, no. 3, pp. 148–151, 2009.

[53] C. M. Watts *et al.*, "Terahertz compressive imaging with metamaterial spatial light modulators," *Nature Photon.*, vol. 8, no. 8 pp. 605–609, 2014.

[54] D. Shrekenhamer *et al.*, "High speed terahertz modulation from metamaterials with embedded high electron mobility transistors," *Opt. Exp.*, vol. 19, no. 10, pp. 9968–9975, 2011.

[55] F. Mesa, M. J. Freire, R. Marqués, and J. D. Baena, "Three-dimensional superresolution in metamaterial slab lenses: Experiment and theory," *Phys. Rev. B, Condens. Matter*, vol. 72, no. 23, 2005, Art. no. 235117.

[56] J. A. Ferrari and C. D. Perciante, "Superlenses, metamaterials, and negative refraction," *J. Opt. Soc. Amer. A, Opt. Image Sci.*, vol. 26, no. 1, pp. 78–84, 2009.

[57] D. Schurig *et al.*, "Metamaterial electromagnetic cloak at microwave frequencies," *Science*, vol. 314, no. 5801, pp. 977–980, 2006.

[58] W. Cai, U. K. Chettiar, A. V. Kildishev, and V. M. Shalaev, "Optical cloaking with metamaterials," *Nature Photon.*, vol. 1, no. 4, p. 224, 2007.

[59] S. Ghafari, M. R. Forouzeshfard, and Z. Vafapour, "Thermo optical switching and sensing applications of an infrared metamaterial," *IEEE Sensors J.*, vol. 20, no. 6, pp. 3235–3241, Mar. 200.

[60] T. Hand and S. Cummer, "Characterization of tunable metamaterial elements using MEMS switches," *IEEE Antennas Wireless Propag. Lett.*, vol. 6, pp. 401–404, 2007.

[61] A. Alu and N. Engheta, "Optical nanotransmission lines: Synthesis of planar left-handed metamaterials in the infrared and visible regimes," *J. Opt. Soc. Amer. B, Opt. Phys.*, vol. 23, no. 3, pp. 571–583, 2006.

[62] Z. Fusco *et al.*, "Non-periodic epsilon-near-zero metamaterials at visible wavelengths for efficient non-resonant optical sensing," *Nano Lett.*, vol. 20, no. 5, pp. 3970–3977, 2020.

[63] T. Zentgraf *et al.*, "Babinet's principle for optical frequency metamaterials and nanoantenna," *Phys. Rev. B, Condens. Matter*, vol. 76, no. 3, 2007, Art. no. 033407.

[64] Y. Chen, B. Ai, and Z. J. Wong, "Soft optical metamaterials," *Nano Converg.*, vol. 7, no. 18, pp. 1–17, 2020.

[65] J. Y. Ou, E. Plum, J. Zhang, and N. I. Zheludev, "An electromechanically reconfigurable plasmonic metamaterial operating in the near-infrared," *Nature Nanotechnol.*, vol. 8, no. 4, pp. 252–255, 2013.

[66] Z. Vafapour and A. Zakery, "New regime of plasmonically induced transparency," *Plasmonics*, vol. 10, no. 6, pp. 1809–1815, 2015.

[67] I. Sersic, M. Frimmer, E. Verhagen, and A. F. Koenderink, "Electric and magnetic dipole coupling in near-infrared split-ring metamaterial arrays," *Phys. Rev. Lett.*, vol. 103, no. 21, 2009, Art. no. 213902.

[68] Q. Zhong, T. Wang, X. Jiang, L. Cheng, R. Yan, and X. Huang, "Near-infrared multi-narrowband absorber based on plasmonic nanopillar metamaterial," *Opt. Commun.*, vol. 458, Mar. 2020, Art. no. 124637.

[69] T. Cao, L. Zhang, R. E. Simpson, and M. J. Cryan, "Mid-infrared tunable polarization-independent perfect absorber using a phase-change metamaterial," *J. Opt. Soc. Amer. B, Opt. Phys.*, vol. 30, no. 6, pp. 1580–1585, 2013.

[70] Z. H. Jiang, S. Yun, F. Toor, D. H. Werner, and T. S. Mayer, "Conformal dual-band near-perfectly absorbing mid-infrared metamaterial coating," *ACS Nano*, vol. 5, no. 6, pp. 4641–4647, 2011.

[71] M. Oh, E. Carlson, and T. E. Vandervelde, "Design of an all-semiconductor selective metamaterial emitter in the mid-IR regime with larger feature sizes for thermophotovoltaic energy conversion applications," *J. Electron. Mater.*, vol. 49, no. 6, pp. 1–8, 2020.

[72] F. B. Barho, F. Gonzalez-Posada, L. Cerutti, and T. Taliercio, "Heavily doped semiconductor metamaterials for mid-infrared multispectral perfect absorption and thermal emission," *Adv. Opt. Mater.*, vol. 8, no. 6, 2020, Art. no. 1901502.

[73] F. M. Wang, H. Liu, T. Li, Z. G. Dong, S. N. Zhu, and X. Zhang, "Metamaterial of rod pairs standing on gold plate and its negative refraction property in the far-infrared frequency regime," *Phys. Rev. E, Stat. Phys. Plasmas Fluids Relat. Interdiscip. Top.*, vol. 75, no. 1, 2007, Art. no. 016604.

[74] Z. Vafapour, "Slow light modulator using semiconductor metamaterial," *Proc. SPIE*, vol. 10535, Feb. 2018, 105352A, doi: 10.1117/12.2292259.

[75] A. Ishikawa, T. Tanaka, and S. Kawata, "Magnetic excitation of magnetic resonance in metamaterials at far-infrared frequencies," *Appl. Phys. Lett.*, vol. 91, no. 11, 2007, Art. no. 113118.

[76] H. T. Chen, W. J. Padilla, J. M. Zide, A. C. Gossard, A. J. Taylor, and R. D. Averitt, "Active terahertz metamaterial devices," *Nature*, vol. 444, no. 7119, pp. 597–600, 2006.

[77] W. Withayachumnankul and D. Abbott, "Metamaterials in the terahertz regime," *IEEE Photon. J.*, vol. 1, no. 2, pp. 99–118, Aug. 2009.

[78] N. K. Grady *et al.*, "Terahertz metamaterials for linear polarization conversion and anomalous refraction," *Science*, vol. 340, no. 6138, pp. 1304–1307, 2013.

[79] X. He, "Tunable terahertz graphene metamaterials," *Carbon*, vol. 82, pp. 229–237, Feb. 2015.

[80] R. Sarkar, K. M. Devi, D. Ghindani, S. S. Prabhu, D. R. Chowdhury, and G. Kumar, "Polarization independent double-band electromagnetically induced transparency effect in terahertz metamaterials," *J. Opt.*, vol. 22, no. 3, 2020 Art. no. 035105.

[81] C. Zhang *et al.*, "Nonlinear response of superconducting NbN thin film and NbN metamaterial induced by intense terahertz pulses," *New J. Phys.*, vol. 15, no. 5, 2013, Art. no. 055017.

[82] M. Šindler *et al.*, "Far-infrared electrodynamics of thin superconducting NbN film in magnetic fields," *Superconductor Sci. Technol.*, vol. 27, no. 5, 2014, Art. no. 055009.

[83] C. H. Zhang *et al.*, "Low-loss terahertz metamaterial from superconducting niobium nitride films," *Opt. Exp.*, vol. 20, no. 1, pp. 42–47, 2012.

[84] C. H. Zhang *et al.*, "Terahertz nonlinear superconducting metamaterials," *Appl. Phys. Lett.*, vol. 102, no. 8, 2013, Art. no. 081121.
[85] S. D. Brorson, R. Buhleier, J. O. White, I. E. Trofimov, H. U. Habermeier, and J. Kuhl, "Kinetic inductance and penetration depth of thin superconducting films measured by THz-pulse spectroscopy," *Phys. Rev. B, Condens. Matter*, vol. 49, no. 9, pp. 6185–6187, 1994.
[86] R. Matsunaga and R. Shimano, "Nonequilibrium BCS state dynamics induced by intense terahertz pulses in a superconducting NbN film," *Phys. Rev. Lett.*, vol. 109, no. 18, 2012, Art. no. 187002.
[87] W. Siemons *et al.*, "Dielectric-permittivity-driven charge carrier modulation at oxide interfaces," *Phys. Rev. B, Condens. Matter*, vol. 81, no. 24, 2010, Art. no. 241308.
[88] A. Alipour, A. Farmani, and A. Mir, "High sensitivity and tunable nanoscale sensor based on plasmon-induced transparency in plasmonic metasurface," *IEEE Sensors J.*, vol. 18, no. 17, pp. 7047–7054, Sep. 2018.
[89] Z. Chen, L. Yuan, G. Hefferman, and T. Wei, "Terahertz fiber Bragg grating for distributed sensing," *IEEE Photon. Technol. Lett.*, vol. 27, no. 10, pp. 1084–1087, May 15, 2015.
[90] H. Liu, G. Ren, Y. Gao, Y. Lian, Y. Qi, and S. Jian, "Tunable subwavelength terahertz plasmon-induced transparency in the InSb slot waveguide side-coupled with two stub resonators," *Appl. Opt.*, vol. 54, no. 13, pp. 3918–3924, 2015.
[91] Y. Shahamat and M. Vahedi, "Mid-infrared plasmonically induced absorption and transparency in a Si-based structure for temperature sensing and switching applications," *Opt. Commun.*, vol. 430, pp. 227–233, Jan. 2019.
[92] S. Weng, L. Pei, J. Wang, T. Ning, and J. Li, "High sensitivity D-shaped hole fiber temperature sensor based on surface plasmon resonance with liquid filling," *Photon. Res.*, vol. 5, no. 2, pp. 103–107, 2017.
[93] N. Luan, C. Ding, and J. Yao, "Refractive index and temperature sensing based on surface plasmon resonance and directional resonance coupling in a PCF," *IEEE Photon. J.*, vol. 8, no. 2, Apr. 2017, Art. no. 4801608.
[94] L. Xia *et al.*, "Graphene based terahertz amplitude modulation with metallic tortuous ring enhancement," *Opt. Commun.*, vol. 440, pp. 190–193, Jun. 2019.
[95] V. Sorathiya, S. K. Patel, and D. Katrodiya, "Tunable graphene-silica hybrid metasurface for far-infrared frequency," *Opt. Mater.*, vol. 91, pp. 155–170, May 2019.

Zohreh Vafapour (Member, IEEE) received the B.Sc. degree in applied physics from the University of Hormozgan, Iran, in 2008, and the M.Sc. degree in condense matter physics and the Ph.D. degree in physics, optics and laser from Shiraz University, in 2011 and 2016, respectively. From July 2014 to December 2014, she was a Visiting Ph.D. Student with the Electrical and Computer Engineering Department, The State University of New York at Buffalo, Buffalo, NY, USA. Since 2016, she has been a Postdoctoral Fellowship with The Johns Hopkins University. She was a Ph.D. and M.Sc. Advisor of Physics and Electrical Engineering Students. She joined the Electrical and Computer Engineering Department, The University of Illinois at Chicago, and the Bio Engineering Departments, The University of Illinois at Chicago. She has hosted and participated in more than seven national and international research projects. She has authored or coauthored 25 peer-reviewed journal articles and 23 conference papers. Her research interests include optical and photonics designs/devices, plasmonics, metamaterials, optical and biomedical sensors, optical antennas, and laser cooling of semiconductors. She is an Active Member of the Optical Society of America.

Mitra Dutta (Life Fellow, IEEE) received the Ph.D. degree from the University of Cincinnati, Cincinnati, OH, USA, in 1981. She is currently the Vice Chancellor for Research and a University Distinguished Professor with the University of Illinois at Chicago, Chicago, IL, USA. She is also a Professor of Electrical and Computer Engineering and an Adjunct Professor of Physics with the University of Illinois at Chicago. She has published in engineering and the physical sciences about 340 journal articles, coauthored two books, 30 patents, and coedited four books. She is a Fellow of the American Association for the Advancement of Science, a Fellow of the Optical Society of America, a Fellow of the American Physical Society, and the Emeritus of the Army Research Laboratory. She received the 2000 IEEE-USA, Harry Diamond Memorial Award, and the 2003 National Achievement Award of the Society of Women Engineers.

Michael A. Stroscio (Life Fellow, IEEE) received the Ph.D. degree from Yale University, New Haven, CT, USA, in 1974. He is currently a University Distinguished Professor, Richard and Loan Hill Professor of Engineering, a Professor of Bioengineering, a Professor of Electrical and Computer Engineering, and an Adjunct Professor of Physics with the University of Illinois at Chicago, Chicago, IL, USA. He has published in engineering and the physical sciences about 450 refereed articles, coauthored four books, more than 12 patents, and coedited five books. He is a Fellow of the American Association for the Advancement of Science, the American Physical Society, the American Institute of Medical and Biological Engineering, the Yale Science and Engineering Association, and the Emeritus of the Army Research Laboratory. He received the 1998 IEEE-USA Harry Diamond Memorial Award.